Eur. Phys. J. B (2022) 95:130
https://doi.org/10.1140/epjb/s10051-022-00392-z

THE EUROPEAN PHYSICAL JOURNAL B

Regular Article - Solid State and Materials

Conduction properties of semiconductive multiwalled carbon nanotubes

M. Ahlskog[1,a], O. Herranen[1,2], J. Leppäniemi[1,3], and D. Mtsuko[1,4]

[1] Department of Physics and Nanoscience Center, University of Jyvaskyla, 40014 Jyvaskyla, Finland
[2] Present Address: Trioptics Scandinavia Oy, Tampere, Finland
[3] Present Address: VTT Technical Research Centre of Finland Ltd., Espoo, Finland
[4] Present Address: Philips MEMS and Micro Devices, Eindhoven, The Netherlands

Received 20 June 2022 / Accepted 1 August 2022 / Published online 13 August 2022

Abstract. We have undertaken low-temperature conduction measurements on arc-discharge synthesized, semiconducting multiwalled carbon nanotubes (MWNT). The diameters of these are in the range 2.5–10 nm, corresponding to the sizes just above single-walled carbon nanotubes (SWNT), up to middle-sized MWNTs. The energy gap, inversely related to the diameter, varies strongly in this range, and consequently there is a strong dependence of the transport on tube diameter. Certain transport characteristics are much alike those found in SWNTs, such as the ON-state resistance and Coulomb blockade. However, the transport gap has a more complex behavior than the corresponding one in semiconducting SWNTs, and a number of features, such as negative differential resistance are commonly observed. Different models for the small bias transport behavior are briefly discussed, and we consider especially the possibility of conduction via the second layer.

1 Introduction

The electronic transport properties of single multiwalled carbon nanotubes (MWNT) have been intermittently studied since the emergence of carbon nanotubes (CNT) in the early 90s [1]. The results are still somewhat fragmentary, especially when compared with the successful work performed on single wall carbon nanotubes (SWNT) [2, 3].

In practice, the transport properties of a MWNT have mainly been equated with that of the outer layer, as almost without exception the microelectrodes make contact to that one. In high-quality MWNTs, the different layers are cleanly separated by the well-known van der Waals gap of about 3.4 Å [4], which significantly limits interlayer interaction. Arc-discharge grown MWNTs (or comparable MWNTs) exhibit a relatively good structural order, and can thus be classified as high-quality MWNTs. Hence, they are typically used in experiments that strive as close as possible to the ideal behavior of MWNTs [5].

Our previous experimental work on transport in single small diameter (< 10 nm) MWNTs [6, 7] has demonstrated the division between metallic characteristics and semiconductivity in MWNTs, which previously was much less clear as among SWNTs. Metallic low bias conduction in a well-conducting MWNT is well explained as taking place solely via the outer layer, due to the above-mentioned low interlayer conductance. Several groups have experimentally explored such MWNTs, where usually the diameter has been over 10 nm. Mainly diffusive, sometimes quasiballistic metallic states have been reported in these [7–10]. Such experiments are also important, where a very strong axial magnetic field can tune the energy gap of a semiconducting outer layer, which is possible in the larger MWNTs, with a much bigger cross-section compared with the SWNT [11, 12].

A few specific works [5, 13] have experimentally explored the interlayer conduction in MWNTs, but more systematic efforts to treat interlayer transport phenomena, both experimentally and theoretically, have exclusively concentrated on the most simple case, which is the double wall carbon nanotube (DWNT) [14]. Till date, however, experimental work shows that in practice the DWNT has quite similar transport properties as the SWNT, though the fundamental difference between the two does of course show up in some situations [15]. Moreover, the conditions for interlayer tunnelling necessarily change as the tube diameter grows, and therefore, concerning transport properties, the DWNT is poorly representative of MWNTs in general.

Supplementary Information The online version contains supplementary material available at https://doi.org/10.1140/epjb/s10051-022-00392-z.

[a] e-mail: ahlskog@jyu.fi (corresponding author)

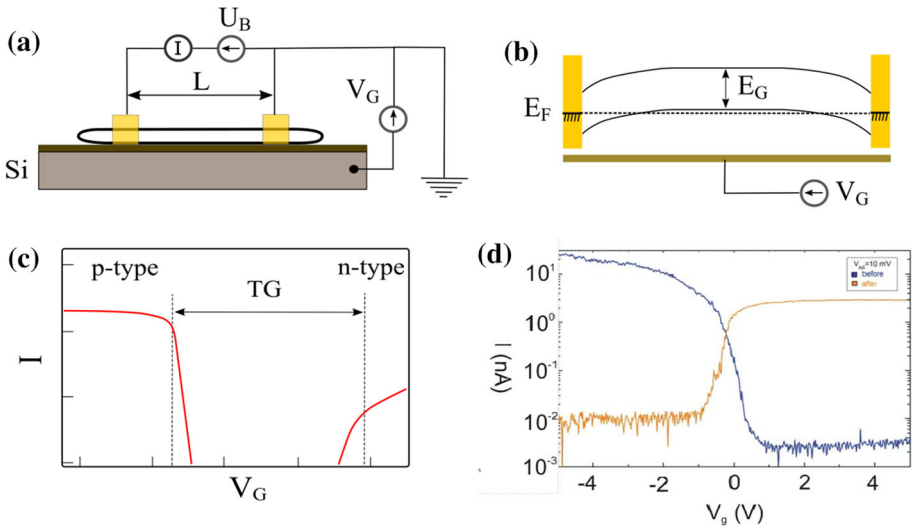

Fig. 1 **a** The typical measurement setup, for conduction measurement of a SWNT on a FET structure with a backgate electrode. Device length is L. **b** A scheme of the energy bands of a semiconducting SWNT as influenced by the electric field from a backgate electrode, where the gate voltage V_G is applied. **c** A schematic drawing of the typical gate curve, of a semiconducting SWNT/CNT. **d** Gate curves of a pristine SWNT (blue), in practice oxygen doped and exhibiting p-type behavior, which after doping with dissolved lithium, a strong reducing agent, turns to n-type behavior (yellow) [16]

The picture of the MWNT as that of a single outsized SWNT, which is mechanically supported by an electronically inert interior structure, evidently is often quite sufficient for metallic cases. In the case of a semiconducting outer layer, the problem is more complicated, as there is less obvious reason to ignore the inner layers. In this work, we look closer on the transport properties of semiconducting MWNTs.

As there is very solid work on semiconducting SWNTs, we review it as a background to the transport measurements on our MWNT devices. The central transport measurement for a single CNT is performed in a field-effect transistor (FET) configuration with a backgate electrode, depicted schematically in the case of the SWNT in Fig. 1a (further details in the Supplement).

The cumulative experience shows, that the SWNTs are slightly p-type due to oxygen doping, and that the work function level of the common electrode metals (Au, Pd) places the SWNT valence band edge closer to the Fermi-level (E_F) [17]. In Fig. 1b is shown how the valence- and conduction bands of a semiconducting SWNT might connect to the metal electrodes. According to the prevailing conception, Schottky-type barriers are formed within the SWNT, at the tube-electrode contacts. These barriers effectively add to the contact resistance, and easily dominate it.

By adjusting the gate voltage V_G, the Fermi-level in the SWNT shifts, and thus the Schottky-barrier as well, leading to very different charge carrier transport conditions from the metal electrodes to the main body of the tube, from low resistive carrier injection (the "ON" state) to tunneling over a maximized Schottky barrier ("OFF" state). In very clean, ballistic SWNTs, the ON-state of semiconducting tubes, as well as metallic cases, have very closely the quantized resistance: $h/4e^2 = 6.5\ \mathrm{k\Omega}$.

In Fig. 1c is shown schematically the central features of a gate curve that typically result as the gate voltage is swept over a large range. The OFF-state in a semiconducting CNT corresponds to a gate voltage range when both electron (n-type conduction) and hole injection (p-type) face a Schottky barrier. The OFF-state range is also called the transport gap (TG) in the gate curve. The boundary between the ON- and OFF-states, is rather simple in the case of SWNTs [17]. If the TG is directly connected with an energy gap (as in Fig. 1b), the conductance falls smoothly with a sharpness which is determined by temperature and magnitude of E_G.

As depicted in Fig. 1c, usually the ON-state on the p-type side (negative V_G), has a stronger conduction than that on the n-type side. This is interpreted as a consequence of the situation in Fig. 1b, in which the Fermi-level is much closer to the valence band in the bulk of the tube. In fact, often the n-type conduction might not appear at all within the experimental gate voltage range for a typical SWNT with an $E_G > 0.5$ eV. Figure 1d shows data on a SWNT-FET where this is the case (blue curve). A few experiments have been undertaken on SWNTs, in which via chemical doping the Fermi-level has been shifted closer to the conduction band, and whereby doping changes radically the gate curve of the SWNT, from p-type to n-type, as shown in Fig. 1d.

Much of the work done on semiconducting SWNTs lacks to date comparable studies in the case of MWNTs. One reason is, that for MWNTs the common synthesis methods produce tubes with diameters (D) mostly above 10 nm whereby the possible energy gap becomes very small. In our previous work on high quality MWNTs with $D < 10$ nm, we found a majority to be semiconducting, and demonstrated an expected inverse D-dependence of E_G, which in turn shows up in the

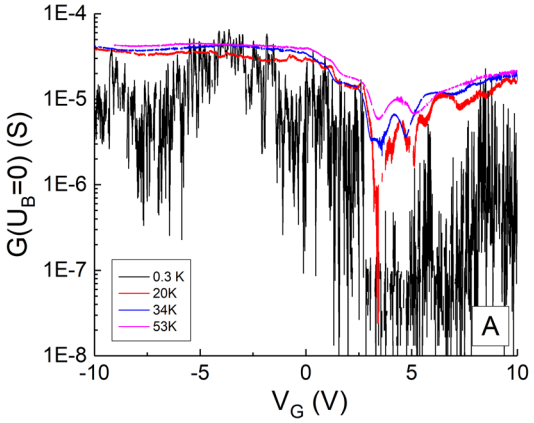

Fig. 2 Temperature-dependent gate curves for a semiconducting MWNTs of $D = 8$ nm (sample A of Table 1). In this case, we exceptionally measured conductance G with lock-in techniques

Table 1 The measured MWNT devices presented in this work

Sample	Figure	D (nm)/L (μm)
A	2, 5, 7, 8	8/1.35
B	3	5/0.8
C	4	2.5/0.6
D1	4	5.5/0.4
D2	6	5.5/0.43
E	4	6.5/0.2
F1	9, 10	5/0.3
F2	–	5/0.6

The left column has sample label, the middle column figures in which the data is presented and the right column the diameter (D) and length (L) of the devices. Samples D and F are MWNTs that have three electrodes and make up two devices each (Supplement)

TG [7]. Figure 2 shows gate curves at different temperatures in a typical case of 8 nm diameter (sample A of Table 1). The TG is smeared out at room temperature, indicating a rather small energy gap. Within the D-range of 2–10 nm, which is of interest to us, E_G's have values roughly in the range 10–100 meV.

In the previous work, we treated the TG as a relatively simple feature of the gate curve, similar as in semiconducting SWNT devices. However, instead of the simple boundary with a smoothly falling conductance in the TG of a SWNT that is described in Fig. 1c, there is more complex behavior in the TG of a MWNT. We already reported in an early work [6] on semiconducting MWNT's the phenomenon of negative differential resistance (NDR), which associates with the TG. However, but for the above-mentioned work on magnetic field effects on the bandgap, the issue of semiconducting transport in MWNTs is a poorly explored topic.

In this work, we present an experimental study on low-temperature transport properties of semiconducting MWNTs, where the focus is on the detailed conduction behavior within their TG. The range of diameters in our MWNTs, 2–10 nm, covers that range where the energy gap changes the most, and should thus be of great interest. We discuss the experimental results and consider what they tell about the different possible transport mechanisms of the MWNT.

2 Experimental

We used solely MWNTs of high quality, conventional arc-discharge synthesized MWNTs, or, in most cases such as were similar to these but synthesized as reported in Ref. [18]. All MWNTs were of diameter below 10 nm. Single MWNT-FET devices were fabricated following standard electron beam lithography procedures where microelectrodes, acting as drain- and source connections, attach to individual MWNTs. The tubes are on pieces of Si/SiO_2 wafer, where the highly doped Si acts as a backgate electrode, separated from the tube by the SiO_2 layer of 300–500 nm thickness (Fig. 1a). Careful AFM imaging was performed on all measured MWNTs to ensure that the outer layer was clean and continuous (at least within the measured section). Altogether, more than 80 MWNTs were measured at low temperatures, though much less have undergone a full investigation. All measurement data presented here has been taken at 4.2 K, unless stated otherwise. The fabrication and conductivity measurement methods are described in more detail in the Supporting Information.

3 Results

3.1 The transport gap in MWNTs of different diameter

Table 1 lists diameter and device length (Fig. 1a) on the MWNT samples to be presented in this work.

We briefly recapitulate the main features of a semiconducting MWNT, more thoroughly presented in Ref. [7], as a necessary basis for this work. In Fig. 2, the p-side ON-state resistance is typically small, about 10–20 kΩ, and its temperature dependence very weak, which is representative for the majority of the samples. This testifies of the relatively small impurity or disorder potential in these MWNTs. We denote in the TG, for the purpose of this discussion, a central region where the conductance is unmeasurably low, and edge regions

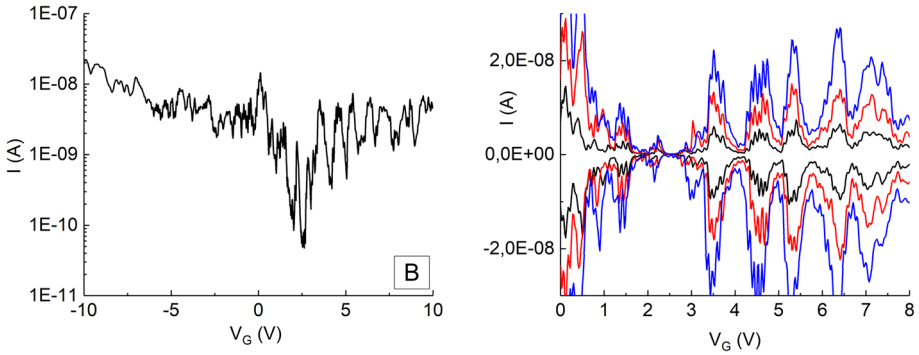

Fig. 3 Left: the gate curve, with current in logarithmic scale, of a typical semiconducting MWNT sample B. $U_B = 1$ mV. Right: close up of the gate curve, in linear scale, at the transport gap (TG) at different bias voltages. $U_B = -3$ mV ... $+3$ mV, in 1 mV steps (zero curve is absent)

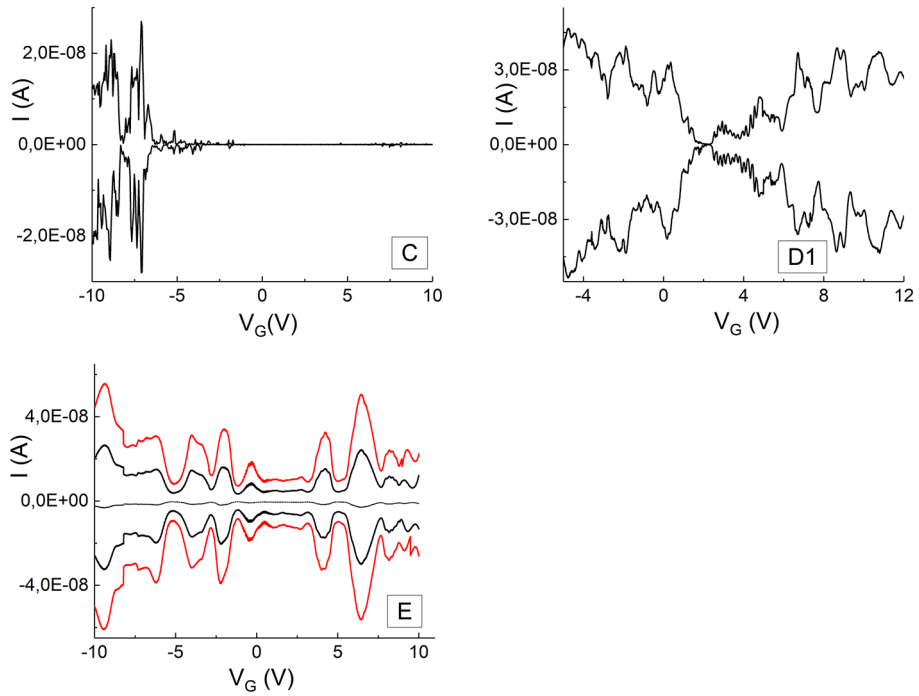

Fig. 4 Clockwise from top left: two examples of gate curves in semiconducting MWNT devices with small (C) and moderate (D1) diameter. $U_B = \pm 1$ mV. Sample E is an example of a MWNT device with quasimetallic gate curve. $U_B = -2$ mV ... $+2$ mV, in 1 mV steps

on either side of the central part of the TG, where the conductance rises, often very unevenly, to the level of the ON-state.

The entire TG in the typical semiconducting MWNT has a nonuniform shape, as the edge region on the p-type side of the gate curve is much sharper than that on the n-type side. Moreover, in a rough approximation, on the n-type side the ON-state resistance is larger, up to by a factor of 10, than on the p-side. The TG is also dependent on the device length (L), as is extensively discussed in the previous work [7] and briefly in the Supplement of this work. These features are in line with the standard picture of the SWNT-FET, explained in the Introduction, in which the Fermi level is close to the valence band edge.

In the left-hand side graph of Fig. 3 is shown the complete gate curve of another MWNT device (sample B). It is shown in the customary logarithmic scale for the bias current, which is efficient for displaying the TG for a semiconducting CNT. In the right hand side graph is a close-up of the TG at both positive and negative biases, and thus with linear current scale. This presentation style emphasizes some relevant features, as we will see shortly.

Figure 4 presents close-up views of the TG of three other different cases, which together demonstrate the variety of the TG among MWNTs with diameter below 10 nm. Samples C and D1 have diameters relatively small ($D = 2.5$ nm), or moderate ($D = 5.5$ nm), respectively. The former conducts appreciably only at the p-side (negative V_G), of a rather large gate voltage range, which is expected with a large E_G (on the order of 0.1 eV) in small diameter tubes. On the other hand, device D1, with larger diameter and smaller E_G (on the order of 10 meV), exhibits a finite conductance almost throughout the gate voltage range.

Although in the graph even the central part of the TG of D1 seems to have an appreciable conductance, a narrow segment of the gate curve would have an unmeasurably high zero-bias resistance in the low temperature limit. As opposed to this, quasimetallic samples are such where a real gap is not observed in this sense. In sample E, the zero-bias resistance maximum in the

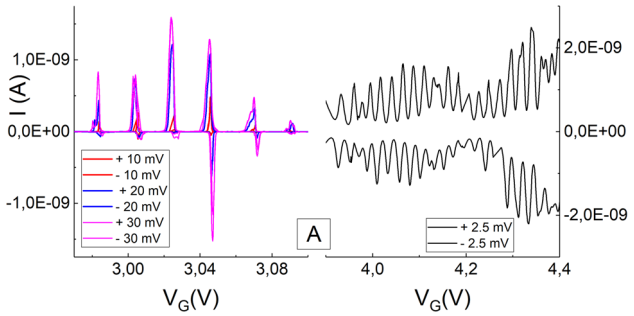

Fig. 5 In Sample A, data from two different small voltage ranges of the gate curve, that exhibit Coulomb blockade. On the left, is a range which is relatively close to the TG center, while the one to the right is well off the center. U_B is given for both graphs in its Label box

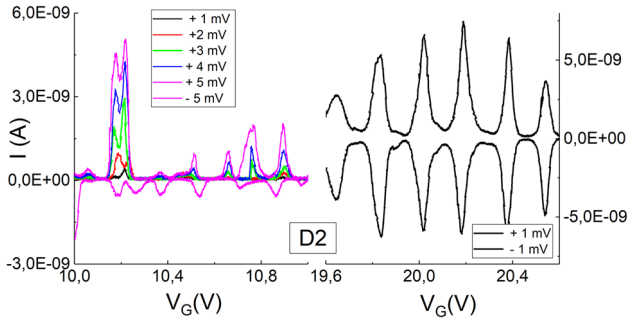

Fig. 6 Sample D2, similar data as in Fig. 5

center of the TG is around 0.1 MΩ. The quasimetallic cases are rather few among all of our devices, and might just have a very small energy gap, which is not observable even at 4 K. In this work, we mainly concentrate on devices corresponding to sample D1 (incl. devices A and B) which represent the majority of the measured devices.

In MWNT devices like D1 above, the conductance at the edge region of the TG is typically dominated by a modulation factor. As in sample B, it is often more apparent on the n-type side, where the conductance changes less sharply than on the p-type side. The situation is quite clearly different from semiconducting SWNTs, where the boundary of the TG does not exhibit similar modulation behavior. As a rough description, the modulation appears in the section of the gate curve when the (zero bias) resistance falls from the ON-state value (typically 10–20 kΩ), to values on the order of 1 MΩ, and with a semiregular period ΔV_G = 2–5 V. For the ensuing discussion, we can note from the data, that it is reasonably symmetric with respect to bias (U_B) polarity.

3.2 Coulomb blockade oscillations

Next, we move to finer features of the gate curve, namely Coulomb blockade oscillations, which are well known from SWNT devices. In Figs. 5 and 6, on the right-side graph, are shown typical such oscillations that stems from a gate voltage range in the n-type edge region of the TG. Regular Coulomb blockade oscillations occur in some cases for quite long gate voltage ranges, such have typically values of 20–50 mV for the oscillation period. The values are rather similar to those observed in SWNT devices. We observe at best a single, clear period with uniform amplitude, but usually varying degree of disorder to this pattern. There are few signs for a more complex, but well-ordered structure in the Coulomb blockade pattern, as is seen in so-called ultraclean SWNT devices [3].

We can analyze the Coulomb blockade oscillations by applying conventional electrostatics as is usual in SWNT devices [17]. The capacitance C of a CNT, separated by a gate insulator of thickness h from a planar counterelectrode, can be estimated as $C/L = 2\pi\varepsilon\varepsilon_0/\ln[4h/D]$. When calculated for the values that occur in our situation, where h is of the order of 0.5 μm, a C/L value of the order of 10 aF/μm is obtained. This corresponds reasonably well (given the rough estimates) to the measured oscillation period since Δ_{CB} estimated as e/C yields e/10 aF = 16 mV. We present in the Supplement some further analysis on how Coulomb blockade depends on device length and bias voltage.

The results presented above were concerned with Coulomb oscillations in the edge regions of the TG (typically n-type side). At locations closer to the TG center the situation changes, as can be seen in the left-hand side graphs in Figs. 5 and 6. These Coulomb oscillations are much more irregular and a profound asymmetry with respect to bias voltage appears.

We can put this asymmetry into sharp perspective by recalling sample E in Fig. 4, in which the conductance is symmetric throughout the TG. The discernible asymmetry in this kind of sample is small and probably attributable either to technical factors or sample properties that are insignificant in this context. These cases, however, are rather few, they are quasimetallic or have a very small gap, with resistance level low (< 1 MΩ) even in the center of the TG.

3.3 Other conduction phenomena within the transport gap

To take a closer look on the bias dependence, and possible asymmetry, in the central part of the TG, Fig. 7 shows such gate curves in an ordinary case, sample A. The three graphs show with increasing detail in gate and bias voltage, how the asymmetry becomes dominant as one restricts the view to the central region of the TG. Switching polarity between source and drain electrodes does not affect the asymmetry, from which we may conclude that asymmetric structural features (that would have evaded from us during fabrication) does not lie behind the effect.

Moreover, another property is visible in the third graph of Fig. 7 (also barely in the previous one): one can see that occasionally the gate curves cross each other,

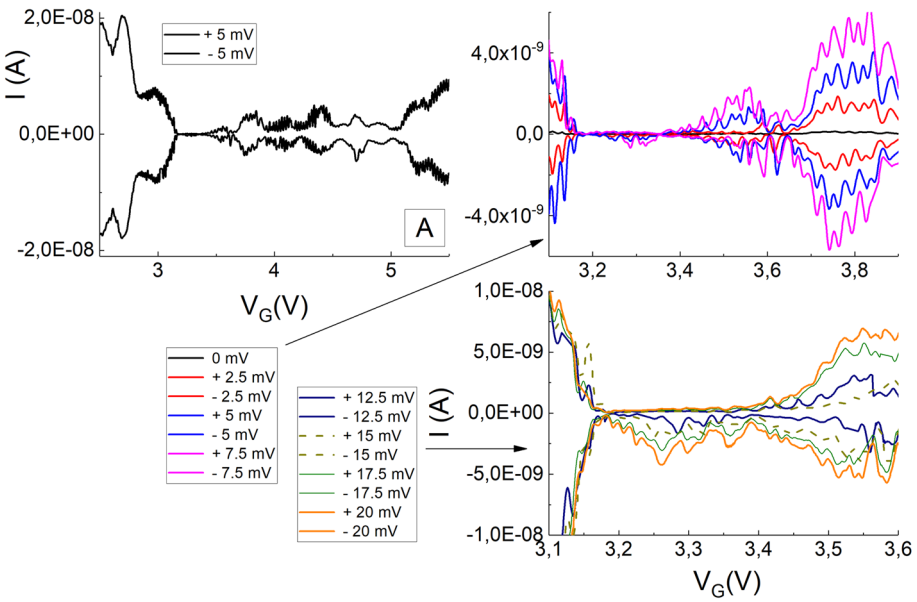

Fig. 7 Gate curves of sample A. Clockwise from the top left graph, the central part of the TG is shown in greater detail, and with a larger range of bias voltage. U_B is given for each graphs in its Label box

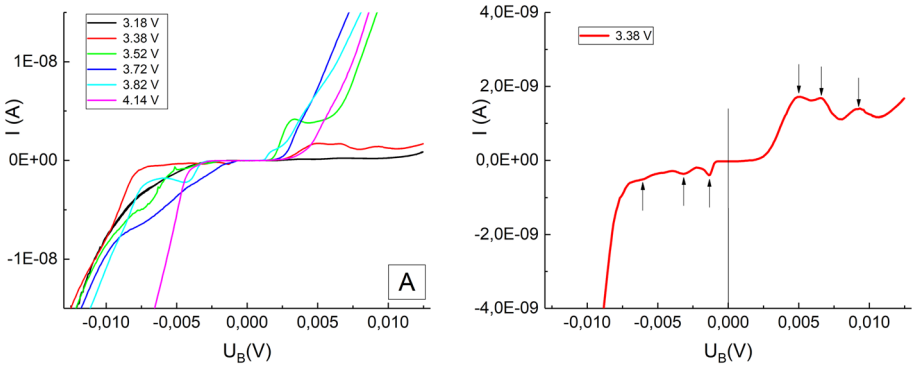

Fig. 8 Left: IV-curves of the sample A in Fig. 8, measured at the gate voltages indicated at each respective IV-curve. Right: the IV-curve at V_G = 3.38 V shown in greater detail. The vertical line helps to locate the zero point of the IV-curve and thus the asymmetry

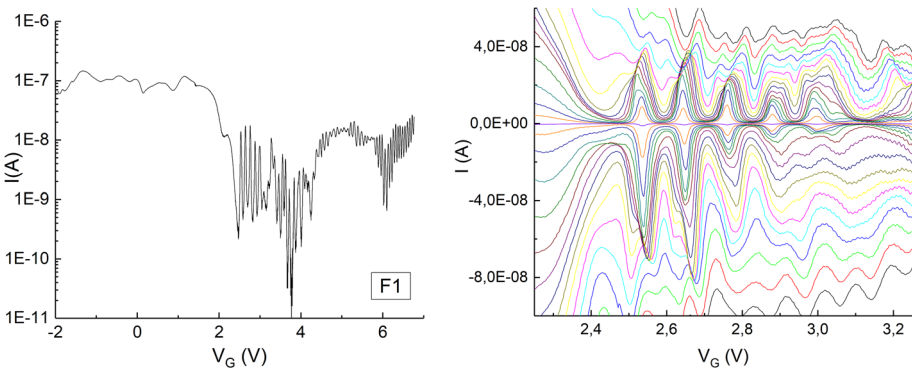

Fig. 9 Left: gate curve of sample F1. U_B = 1 mV. Right: close-up within the central part of the TG. U_B = − 15 mV ... + 15 mV, in 1 mV steps

which means that the device exhibits negative differential resistance (NDR) at certain gate voltages.

Note the slight mismatch in gate voltage dependence of TG, which is apparent when comparing Figs. 5 and 7. This is due to the well known hysteretic shifting of the gate curves, which stems from impurities and defect-related charges in the gate insulator and possibly the CNT itself [19]. The two measurements were performed at different cooling runs, whereby a shift in the position of the TG is understandable, since the hysteresis occurs at temperatures that allow ionic mobility. However, the shift does not appreciably change the form of the TG.

At cryogenic temperatures, the hysteretic effect is mostly negligible, but could be a conceivable source of misinterpretation if very fine features are to be concluded from gate curve-data solely. Valuable complementary data are obtained from IV-characteristics at different gate voltages. Figure 8, left-side graph, shows IV-curves taken from the same sample (as in Fig. 7), at a few gate voltages within the central part of the

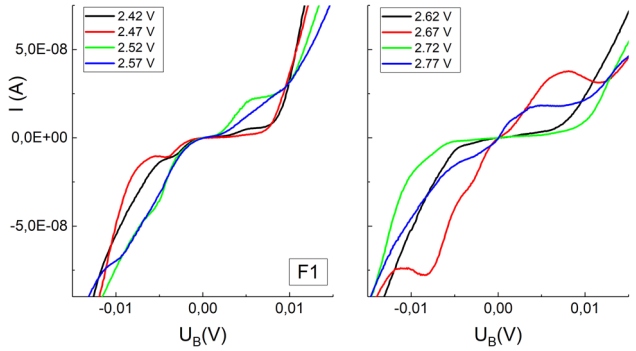

Fig. 10 IV-curves of sample F1 in Fig. 9, measured at the gate voltages indicated in the Label boxes. The data are split into two graphs for the sake of clarity. The current axis of the right graph is identical with that of the left hand side

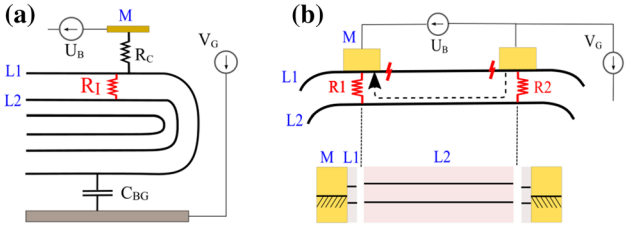

Fig. 11 **a** Schematic representation of the external (black) and internal (red) electronic connections in the MWNT device, explained in the text. The outer connections are as in the SWNT device shown in Fig. 1a. The blue labels denote the metal electrodes (M), the outer layer (L1), and the second layer (L2), and are also used in the b)-figure. **b** Upper image: scheme for current transport in a MWNT (only part of it has been drawn), in which the outer layer (L1) is blocked by gate voltage-induced Schottky-type barriers at the electrodes (M). In this situation, the current flows via the second layer (L2), as indicated by the arrow. Lower image: an energy level diagram that depicts the case of inner layer transport with the Fermi-level in the metal electrode and the band edge energies in L1, and L2. The dashed lines between the upper scheme and the diagram indicate in both the section of L2, which is the device length indicated in Fig. 1a

TG. A variable bias gap (range of U_B with zero current) among the IV-characteristics can be observed. We showed in our previous work, that at a certain gate voltage within the central part of the TG, a maximum bias gap can be extracted, which corresponds to the energy gap of the MWNT, if the device is short and conduction is quasiballistic [7]. Here, the device length ($L = 1.35\ \mu m$) is relatively large and, therefore, the bias gap, on the order of 10 mV, corresponds to an upper estimate for the energy gap of the MWNT.

The asymmetry and NDR is clearly seen in the IV-curves as well, and at the same bias voltage values as expected from the gate curves. The right-hand side graph shows one of the gate curves in greater detail. It exhibits some peaks which are pinpointed with the arrows, and which are rarely seen with this clarity. But for the asymmetry with respect to the zero-point of the IV-curve, the three peaks on either side seem to mirror each other.

Figures 9 shows the basic gate curve for sample F1 (in a little restricted voltage range), and the central section of the TG in much greater detail. Asymmetry and NDR are again visible and can be seen in great detail.

Figures 10 shows for the same sample F1 IV-curves for a few gate voltages and again there is good correspondence with the gate curve data (Fig. 9). Among the IV-curves, are captured some IV-curves with high zero-bias conductance, which correspond to the Coulomb blockade maxima in their respective gate curve data. This high conductance is in resistance on the order of 100 kΩ. The NDR maxima occur at similar magnitudes of voltage as the bias gap and occur at both positive and negative bias voltages. The effect seems to be associated in the IV-characteristics with the asymmetry.

4 Summary of the main results

We can summarize the obtained results as follows. The inverse diameter dependence of the energy gap leads to a strong variation of the TG in semiconducting MWNT devices with diameter below 10 nm, as was demonstrated in Fig. 4. Certain transport characteristics have very close corresponding features in SWNT devices, such as the large-scale features of the TG and Coulomb blockade phenomena. On the other hand, especially those MWNT devices with a modest TG (Fig. 4b) exhibit a number of features that do not find correspondence in SWNTs. These include the large-scale modulation of the resistance in the edge region, which is symmetric with respect to bias polarity, and the asymmetry and NDR in the central part of the TG.

While the above-mentioned characteristic features are prominent in MWNTs with moderate size energy gaps, they are poorly observable if the gap is either small or large. The former are devices in the quasimetallic limit, where the TG does not possess a true gap of infinite zero bias resistance in the low temperature limit. The latter are small diameter tubes, with E_G of the same magnitude as in ordinary SWNTs.

5 Discussion

We have consistently presented our results as either similar to the typical SWNT device, or as something qualitatively different. This relates directly to the question of whether transport processes in a MWNT are a matter solely of the outer layer, or whether there is the possibility of interlayer transport via the second layer.

A MWNT device is connected electrically similarly as the SWNT device of Fig. 1a. An elementary model that describes its electrical behavior is shown in Fig. 11a.

The quantities in black (R_C, C_{BG}) are connections to the outer layer of the MWNT, that are similar with corresponding SWNT devices. R_C is the contact resistance. C_{BG} is the capacitance between the backgate electrode and the outer layer of the MWNT. R_I, in red, connects the space between outer and the second layer, which is the van der Waals gap of 3.4 Å. It stands in this model as the primary correction to the scheme of sole outer layer transport.

The ON-state resistance that we observe is roughly equivalent to that reported for SWNTs, and includes R_C from the model of Fig. 11a. R_C should, therefore, be in the range of 1–10 kΩ. The similarity with SWNT transport also includes the asymmetric shape of the gate curve, with higher p-type conduction and sharper p-type boundary of the TG, as well as the Coulomb oscillations at the edge region of the TG. C_{BG} was estimated from these, and is alike those seen in SWNTs, that is, around 10 aF.

At the edge region of the TG, the Schottky-type barrier in the outer layer between the segment at the metal electrode and the rest of the outer layer becomes dominating in the device resistance. The large-scale modulation of the resistance lacks comparable data in work on SWNTs or DWNTs. In Ref. [20] rather weak steps in room temperature gate curves were reported in SWNT-FETs.

This modulation is proposed to be accounted via the outer layer density-of-states (DOS) of the MWNT, as a factor in the tunnelling conduction over the Schottky-type barrier. The smaller energy scales of that layer, due to the 1/D-dependence, means that the DOS variations could be more readily observable in the MWNT gate curve than in the corresponding SWNT data. The modulation occurs within a characteristic quasiperiod of $\Delta V_G = 2$–5 V. This suggests that a subband is filled or emptied via the capacitance C_{BG} within this period. In a 0.5 μm long MWNT device a single subband could host around 500 electrons. Then we can make the estimate $C_{BG} = 500\ e/\Delta V_G \approx 50$ aF. This value is well in line with other estimates of the capacitance [17].

The resistance modulations within the edge region of the TG thus still fit into the picture with sole outer layer transport. In the central parts of the TG there is a radical change of behavior, as the resistance approaches and exceeds the 1 MΩ level, where the asymmetry and the NDR phenomena sets in. There are very alternative ways to accommodate these phenomena, based on either continuing with a model of sole outer layer transport, or to include conduction via the second layer. A truly reliable model for the electronic transport in a MWNT is beyond the scope of this work, but we present here some viewpoints on the problem.

Within the picture of sole outer layer transport, a model based on multiple quantum dots and Coulomb blockade could be constructed, which could count for some of our observed phenomena. This model has been applied for graphene nanoribbons, where local impurity potentials divide the quasi-one-dimensional conductor, from the point of view of electronic transport, into a series of connected quantum dots [21]. In that case external factors, and not the intrinsic properties of the nanoribbon, determine the transport properties, and each nanoribbon device has individual, non-repeatable, features. As we demonstrate in the Supplement, in our devices two different sections of the same MWNT exhibit similar features, which implies that the conductance pattern connects with the intrinsic bandgap E_G stemming from the chiral structure of the MWNT, which is contrary to the multiple quantum dot picture.

As one speaks of MWNTs in general, it becomes increasingly difficult to ignore the inner layers with increasing diameter. Most of the previously published works on MWNTs have dealt with metallic conduction, whereby the sole-outer layer model will do, due to the high anisotropy. In this work, we deal with semiconducting tubes, and the asymmetry and the NDR observed in these are, at least predominantly, seen only in MWNTs. This would argue for linking these phenomena with interlayer transport.

A starting point for a conceivable model of inner layer transport is the observation, that when the total resistance of the outer layer is very large within the TG, current could flow via the second layer. The scenario with a blocked outer layer is depicted in the upper part of Fig. 11b. Here the resistances R1 and R2 at the electrodes, which are local values for the distributed tunnelling barrier resistance of Fig. 11a, lead the current to and from the second layer. In the figure, the path is depicted with the arrow-headed line.

The most typical case would be that both the outer and second layers are semiconducting. An energy level diagram for this situation is pictured in the lower part of Fig. 11b. The Fermi-level of the metal electrode (M) is typically between the conduction and valence band edges of the outer layer (L1). The narrow space between L1 and L2 purports to illustrate the van der Waals gaps between the two layers, which become the tunneling resistances R1 and R2.

This model resembles the well-known resonant tunnelling diode made from a semiconductor double barrier heterostructure [22]. That one is constituted altogether of two-dimensional layers, while in our case the central island is a μm-scale one-dimensional conductor (L2). But the protected inner layer of a high-quality MWNT could very well have the ability to conduct semiballistic transport over the distance corresponding to the device length.

Resonant tunnelling double barrier heterostructures produce a pronounced NDR effect, and could constitute a distant model for our situation. The NDR phenomenon occurs according to the above-described model when the metal electrode Fermi level aligns with either of the L2 band edges. The finer structure, which is exceptionally well visible in case of Fig. 8, would in this picture reflect the band structure in L2. For estimating the characteristic values for R1 and R2, we recall the sample of Fig. 10, where the minimum resistance within the TG was estimated to be on the order of 100 kΩ. We pointed out in our preliminary work on the NDR effect [6] that one can associate with it a

characteristic resistance range of around 0.1–1 MΩ. In the experimental works of Refs. [5] and [13], values for the intershell resistance on the order of 10 and 100 kΩ were obtained, respectively, where the former were in MWNTs of diameter predominantly over 10 nm, and the latter below it.

Separately, the tunnelling structures R1 and R2 obviously have an asymmetric character. In principle, the complete structure of Fig. 11b should still have a symmetric bias response, but an asymmetric response arises if the two tunnelling structures respond differently. It can be expected that the response of the two tunnelling structures is highly sensitive to minute factors in the local potential environment. The potential distribution from the backgate is uneven as a result of the grounding of the device via either of the electrodes, as depicted in Fig. 11b [23]. Therefore, the two oppositely configured asymmetric tunnelling structures, being separated by a μm-scale distance, could conceivably have an asymmetric voltage response, in line with the observed behaviour within the TG of semiconducting MWNT devices.

6 Conclusion

Our detailed measurements on the transport gap of semiconducting MWNTs has shown that the conductive properties can be divided into those compatible with pure outer layer transport, and such that are possibly explained with conduction via the second layer. The first category has mostly a close resemblance to SWNT transport properties, including the Coulomb oscillations. However, the larger diameter of the MWNT outer layer compared to the SWNT, results in a smaller energy scale for the DOS variations, that in our model shows up in resistance modulations of the MWNT transport gap. The second category of transport properties includes the asymmetric behavior and NDR within the central part of the TG. A tentative model for these suggests transport mechanisms governed by interlayer tunnelling. However, we cannot rule out different models for the transport properties.

The experimental data presented here on the transport behavior of the semiconducting MWNTs is rather plentiful and complex and certainly deserves much further study. Future research will hopefully provide theoretical analysis especially of interlayer transport in MWNTs to have a satisfactory model of MWNT devices. Moreover, we have assumed that the outer and the second layer contribute to the transport as separate entities. The recent activity on bilayer graphene could in the case of one-dimensional Moiré interferences further complicate and enrich the study of MWNTs [24, 25]. The physics of interlayer interactions are at the forefront of current condensed matter physics, and the related case of MWNTs should have new importance as well.

Acknowledgements This work was supported by the Academy of Finland, Grant nr. SA-7122008.

Author contributions

OH, JL, and DM have contributed to sample fabrication, measurements, and data analysis. MA has contributed to data analysis and has written the manuscript.

Funding Open Access funding provided by University of Jyväskylä (JYU).

Data availability statement The data that support the findings of this study are available from the corresponding author upon reasonable request.

References

1. L. Langer, V. Bayot, E. Grivei, J.P. Issi, J.P. Heremans, C.H. Olk, L. Stockman, C. Van Haesendonck, Y. Bruynseraede, Phys. Rev. Lett. **76**, 479–482 (1996)
2. A. Jorio, M. Dresselhaus, G. Dresselhaus (eds.), *Carbon Nanotubes* (Springer, Berlin, 2008)
3. E.A. Laird, F. Kuemmeth, G. Steele, K. Grove-Rasmussen, J. Nygård, K. Flensberg, L.P. Kouwenhoven, Rev. Mod. Phys. **87**, 703 (2015)
4. R. Saito, G. Dresselhaus, M.S. Dresselhaus, *Physical Properties of Carbon Nanotubes* (Imperial College Press, London, 1998)
5. M. Ahlskog, M.J. Hokkanen, D. Levshov, K. Svensson, A. Volodin, Chris van Haesendonck. J. Vac. Sci. Technol. B **38**, 042804 (2020)
6. M. Ahlskog, O. Herranen, A. Johansson, J. Leppäniemi, D. Mtsuko, Phys. Rev. B **79**, 155408 (2009)
7. D. Mtsuko, A. Koshio, M. Yudasaka, S. Iijima, M. Ahlskog, Phys. Rev. B **91**, 195426 (2015)
8. R. Tarkiainen, M. Ahlskog, J. Penttilä, L. Roschier, P. Hakonen, M. Paalanen, E. Sonin, Phys. Rev. B **64**, 195412 (2001)
9. M.R. Buitelaar, A. Bachtold, T. Nussbaumer, M. Iqbal, C. Schönenberger, Phys. Rev. Lett. **88**, 156801 (2002)

10. B. Stojetz, C. Miko, L. Forro, Ch. Strunk, Phys. Rev. Lett. **94**, 186802 (2005)
11. G. Fedorov, P. Barbara, D. Smirnov, D. Jimenez, S. Roche, Appl. Phys. Lett. **96**, 132101 (2010)
12. S.H. Jhang, M. Marganska, Y. Skourski, D. Preusche, M. Grifoni, J. Wosnitza, C. Strunk, Phys. Rev. Lett. **106**, 096802 (2011)
13. B. Bourlon, C. Miko, L. Forro, D.C. Glattli, A. Bachtold, Phys. Rev. Lett. **93**, 176806 (2004)
14. J.-C. Charlier, X. Blase, S. Roche, Rev. Mod. Phys. **79**, 677 (2007)
15. D. Bouilly, J. Cabana, F. Meunier, M. Desjardins-Carriere, F. Lapointe, P. Gagnon, F.L. Larouche, E. Adam, M. Paillet, R. Martel, ACS Nano **5**, 4927 (2011)
16. P. Yotprayoonsak, K. Hannula, T. Lahtinen, M. Ahlskog, A. Johansson, Carbon **49**, 5283 (2011)
17. M.J. Biercuk, S. Ilani, C.M. Marcus, P.L. McEuen, in *Carbon Nanotubes*. ed. by A. Jorio, M. Dresselhaus, G. Dresselhaus (Springer, Berlin, 2008), p.455
18. A. Koshio, M. Yudasaka, S. Iijima, Chem. Phys. Lett. **356**, 595 (2002)
19. M. Shlafman, T. Tabachnik, O. Shtempluk, A. Razin, V. Kochetkov, Y.E. Yaish, Appl. Phys. Lett. **108**, 163104 (2016)
20. J. Appenzeller, J. Knoch, M. Radosavljevic, Ph. Avouris, Phys. Rev. Lett. **92**, 226802 (2004)
21. J. Güttinger, F. Molitor, C. Stampfer, S. Schnez, A. Jacobsen, S. Dröscher, T. Ihn, K. Ensslin, Rep. Prog. Phys. **75**, 126502 (2012)
22. M.J. Kelly, *Low-dimensional semiconductors* (Oxford Science Publications, Oxford, 1995)
23. We measured also the gate curve with a symmetrical grounding arrangement which did not produce a different result.
24. S. Zhao, P. Moon, Y. Miyauchi, T. Nishihara, K. Matsuda, M. Koshino, R. Kitaura, Phys. Rev. Lett. **124**, 106101 (2020)
25. N. Wittemeier, M.J. Verstraete, P. Ordejón, Z. Zanolli, Carbon **186**, 416 (2022)